# Regions associated with electron physics in asymmetric magnetic field reconnection

F. S. Mozer[1] and P. L. Pritchett[2]

Received 24 January 2009; revised 3 March 2009; accepted 6 March 2009; published 3 April 2009.

[1] Spatial relationships between regions containing signatures of electron physics in asymmetric reconnection with a guide field are examined using simulations and space observations that are in excellent agreement. These electron physics regions do not completely overlap, are not confined to sizes ~electron skin depth, and do not surround the X-line. The electron ideal Ohm's law, $\mathbf{E} + \mathbf{U}_e \times \mathbf{B} = 0$, is violated over many ion inertia lengths in the outflow direction. Thus, pressure terms and, to a lesser extent, inertia terms in the Generalized Ohm's Law are important in producing electron physics on ion scales. Parallel electric fields that are necessary but not sufficient for reconnection are found in the simulation and in space on ion scales in the outflow direction. They account for ~10% of $\mathbf{j} \cdot \mathbf{E}$, averaged over the current sheet. The electron exhaust jet exists over a shorter length for asymmetric reconnection than it does for symmetric reconnection. **Citation:** Mozer, F. S., and P. L. Pritchett (2009), Regions associated with electron physics in asymmetric magnetic field reconnection, *Geophys. Res. Lett.*, *36*, L07102, doi:10.1029/2009GL037463.

## 1. Introduction

[2] A goal of magnetic field reconnection research is to understand the site where magnetic field lines from two different topologies reconnect. One or more physical properties have been used to search for this reconnection site [*Vasyliunas*, 1975; *Mozer*, 2005; *Karimabadi et al.*, 2007; *Phan et al.*, 2007; *Shay et al.*, 2007; *Ji et al.*, 2008]. Possible properties of the reconnection site include: (1) A region of size $\sim c/\omega_{pe}$ in which $(\mathbf{E} + \mathbf{U}_e \times \mathbf{B}) \neq 0$ that is embedded in a region of size $\sim c/\omega_{pI}$ where $(\mathbf{E} + \mathbf{U}_I \times \mathbf{B}) \neq 0$, where $\omega_{pe}$ and $\omega_{pI}$ are the electron and ion plasma frequencies, $\mathbf{U}_e$ and $\mathbf{U}_I$ are the electron and ion bulk velocities, and E and $\mathbf{B}$ are the electric and magnetic fields; (2) a non-zero parallel electric field; $\mathbf{E}_{\|}$ (3) a large, spatially confined perpendicular electric field; (4) an electron beta much greater than one; (5) electromagnetic energy conversion, $j \cdot \mathbf{E}$, where $\mathbf{j}$ is the current density; (6) super-Alfvenic electron exhaust flow; (7) a density cavity suggestive of a non-zero divergence of the electron pressure; (8) a current channel of enhanced intensity, suggestive of a non-zero inertia term; (9) electron gyroradius $\leq c/\omega_{pe}$ associated with electron non-gyrotropy; (10) Non-zero heat flux emanating from the region.

[3] The purposes of the present paper are to consider the spatial relationships between some of these regions during asymmetric reconnection, to make the first quantitative comparisons between simulations and space data in such regions, and to emphasize the relative importance of the various terms in the Generalized Ohm's Law. It should be noted that asymmetric reconnection is probably the most prevalent form of reconnection at the sub-solar magnetopause, on the sun, and in all of astrophysics.

[4] It has been shown [*Newcomb*, 1958; *Longmire*, 1963; *Mozer*, 2005] that magnetic field lines moving at the $\mathbf{E} \times \mathbf{B}/B^2$ velocity produce a temporal evolution of the magnetic field identical to that found from Maxwell's equations unless

$$\mathbf{B} \times \left(\nabla \times \mathbf{E}_{\|}\right) \neq 0 \tag{1}$$

Because a pair of magnetic field lines moving towards each other at the $\mathbf{E} \times \mathbf{B}/B^2$ velocity cannot reconnect (they would just pass through each other), equation (1) must be satisfied at the reconnection site. This equation is a necessary but not sufficient condition for reconnection because satisfying it means only that the magnetic field geometry must be obtained from Maxwell's equations. Thus, finite regions where equation (1) is satisfied are candidate regions for reconnection and they have $\mathbf{E}_{\|} \neq 0$. Important parallel electric fields have been observed in space [*Mozer et al.*, 2003; *Mozer*, 2005].

[5] The Generalized Ohm's Law is written in a form convenient for analysis with simulation data as

$$\mathbf{E} + \mathbf{U}_I \times \mathbf{B} = \mathbf{j} \times \mathbf{B}/ne - \nabla \cdot \mathbf{P}_e/ne - (m_e/e) \cdot [\partial \mathbf{U}_e/\partial t + (\mathbf{U}_e \bullet \nabla)\mathbf{U}_e] + \eta \mathbf{j} \tag{2}$$

where n is the plasma density, $\nabla \cdot \mathbf{P}_e$ is the divergence of the electron pressure tensor and $\eta$ is the resistivity. Equivalently, by writing $\mathbf{j} = ne(\mathbf{U}_I - \mathbf{U}_e)$ in the first term on the right side of equation (2), the Generalized Ohm's Law becomes

$$\mathbf{E} + \mathbf{U}_e \times \mathbf{B} = -\nabla \cdot \mathbf{P}_e/ne - (m_e/e)[\partial \mathbf{U}_e/\partial t + (\mathbf{U}_e \bullet \nabla)\mathbf{U}_e] + \eta \mathbf{j} \tag{3}$$

[6] Parallel electric field candidate reconnection regions are also regions in which the left sides of equations (2) and (3) are non-zero. However, these left sides can be non-zero in the absence of parallel electric fields because the perpendicular components of the left sides of equations (2) or (3) can be non-zero in the absence of a parallel electric field. Thus, as will be shown, regions where the ideal Ohm's law is non-zero are larger than the parallel electric field candi-

[1]Space Sciences Laboratory, University of California, Berkeley, California, USA.
[2]Department of Physics and Astronomy, University of California, Los Angeles, California, USA.


0094-8276/09/2009GL037463$05.00

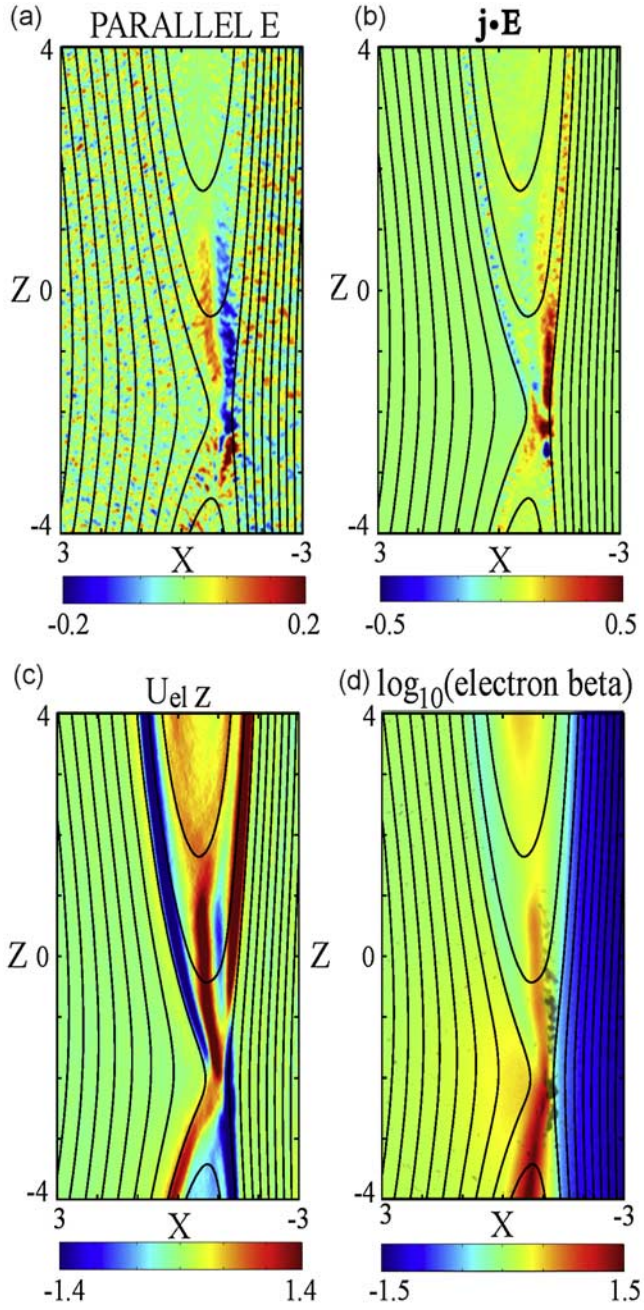


**Figure 1.** The parallel electric field, electromagnetic energy conversion, and electron and ion exhaust outflows in a simulation of asymmetric magnetic field reconnection with a guide magnetic field. The red and blue regions in each plot are the locations where the magnitude of the quantity of interest is greater than half of its peak value.

date reconnection sites and reconnection cannot occur in such larger regions.

## 2. Simulation Model

[7] The PIC simulation model has been described by *Pritchett* [2008]. The asymmetric reconnection configuration is modeled by a hydromagnetic equilibrium in which the Z-component of the magnetic field varies from $-B_0/2$ to $3B_0/2$ from the magnetosheath side to the magnetosphere side and the plasma density varies from $n_0$ to $n_0/10$. A reference velocity, $v_0$, is defined as the Alfven speed based on $B_0$ and $n_0$. The simulation results are presented in dimensionless units in which magnetic fields are normalized as $B/B_0$, electric fields as $E/v_0B_0$, bulk flow velocities as $U/v_0$, current densities as $j/en_0v_0$, and time as $\Omega_{I0}t$, where $\Omega_{I0} = eB_0/m_I$ is the ion cyclotron frequency. The simulation data in this paper is the average over the time interval of 70.25 to 70.5. A single time step in the simulation is 1/2,000 time units.

[8] There is an initial uniform guide magnetic field of magnitude $B_0/2$ directed dawnward, the initial current sheet half-thickness is $c/\omega_{pI}$ (computed using the density $n_0$), and the simulation is driven by a convection electric field $E_Y(z, t)$ imposed on the magnetosheath boundary. This field is ramped up to 0.2 over a time interval of one unit and then held fixed. No local X-line perturbation is imposed. The mass ratio is $m_I/m_e = 200$, $T_I/T_e = 2$, $d_I = c/\omega_{pI} = 40\Delta$ (where $\Delta$ is the grid spacing), and the simulation domain size is $25.6d_I$ by $25.6d_I$. The Z boundaries are open to particles and magnetic flux: particles crossing these boundaries are removed from the system, and new particles are injected at a constant rate based on Maxwellian distributions with temperatures fixed at the initial values.

## 3. Results

[9] Figure 1 presents plots of $\mathbf{E}_{\|}$, $\mathbf{j} \cdot \mathbf{E}$, the electron exhaust velocity, and the electron beta (with the largest $\mathbf{E}_{\|}$ regions superposed in brown) in an 8 by 6 area around the X-line. The plots simulate sub-solar reconnection with X normal to the current sheet and increasing toward the left in the sunward direction and Z in the direction of the reconnecting magnetic fields. The color bars in Figure 1 and in Figures 3 and 4 saturate at half of the peak values of the quantities given by each plot. Thus, the blue and red surfaces in any plot (except electron beta) cover regions in which the absolute value of the quantity of interest is greater than half of its peak value.

[10] The parallel electric fields in Figure 1a have widths in the X-direction of about one electron skin depth and they extend in the Z-direction with magnitudes greater than half of the peak magnitude over at least four ion skin depths. This result is in good agreement with the many direct observations of parallel electric fields in space [*Mozer*, 2005] in that such observations are rather common.

[11] Comparisons between space and simulation results along an X-trajectory through the current sheet are given in Figure 2, in which the normalized simulation quantities are converted to physical units by setting $B_0 = 45$ nT and $n_0 = 10$ cm$^{-3}$. The non-linear X-axes in both columns are approximately scaled by the local electron skin depth. The space data was obtained on the Polar satellite at a magnetopause crossing on April 2, 2002 during a two second interval in which the data was converted from temporal to spatial by assuming that the magnetopause speed was equal to the average value of $(\mathbf{E} \times \mathbf{B}/B^2)_X$ [*Mozer et al.*, 2003]. The simulation data is for a crossing at $Z = -2.28$. Figures 2a and 2b of the space data cover more time than the other plots in order to show the full crossing and to illustrate that

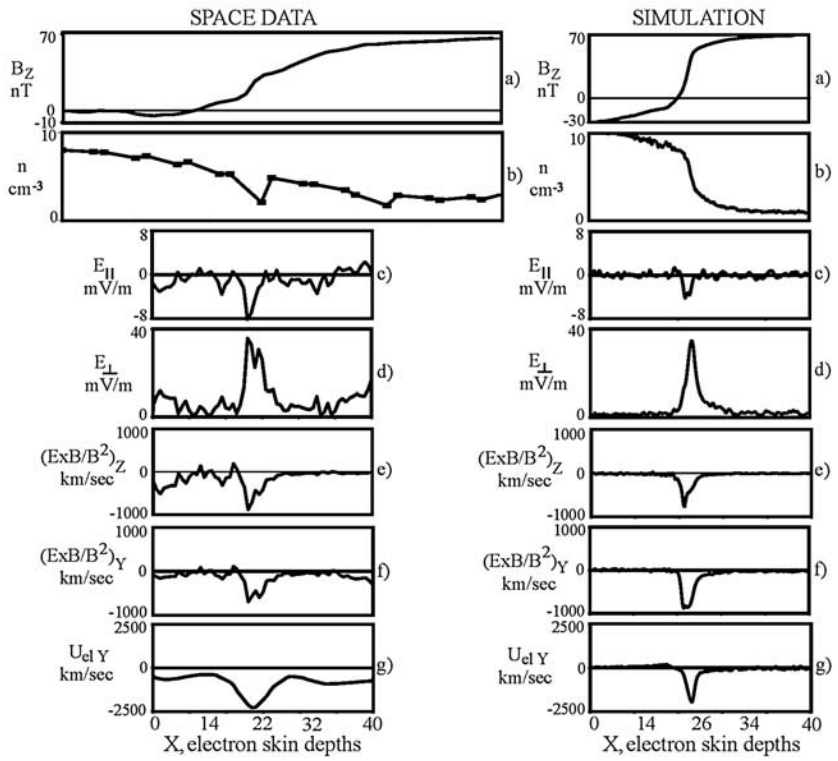


**Figure 2.** Comparison of simulation and space observations of an electron scale region. The guide magnetic field was 22.5 nT in the simulation and 13 nT in the space data.

the minimum variance $B_Z$ for the space data was negative in the magnetosheath, as is required for reconnection to occur. For both data sets, the large slope of $B_Z$ and the rapid change in density near the center of Figures 2a and 2b signify a strong current channel and the possible divergence of the pressure tensor. Thus, the current and pressure terms on the right sides of equations (2) and (3) may be associated with the Figure 2 parallel electric field in Figure 2c the perpendicular electric field in Figure 2d and the large $\mathbf{E} \times \mathbf{B}/B^2$ and electron out-of-plane flows in Figures 2e–2g. It is important to note that the amplitude scales of all identical plots in the two columns are equal, which illustrates the similar magnitudes of the space and simulation quantities. The quantities were large over a width of one or a few electron skin depths. The Y-components of the $\mathbf{E} \times \mathbf{B}/B^2$ velocities in Figure 2f, while large, were smaller than the electron flows in the Y-direction, given in Figure 2g, so the electrons traveled faster than the $\mathbf{E} \times \mathbf{B}/B^2$ velocity to provide the current associated with the variation of $B_Z$. Thus, this event occurred in a region where $\mathbf{E} + \mathbf{U}_e \times \mathbf{B} \neq 0$, as discussed in connection with Figure 3. For the space data, the Y-component of the electron velocity was computed from the slope of $B_Z$ in Figure 2a, while all other quantities were directly measured in space or computed in the simulation.

[12] The electromagnetic energy conversion, $\mathbf{j} \cdot \mathbf{E}$, is illustrated in Figure 1b, in which the blue and red regions are locations where $\mathbf{j} \cdot \mathbf{E}$ is greater than half of its peak magnitude. Again, significant energy conversion of both signs occurs over distances of several ion skin depths in the Z-direction and ~1–2 electron skin depths in the X-direction and along the separatrices. Because the energy conversion

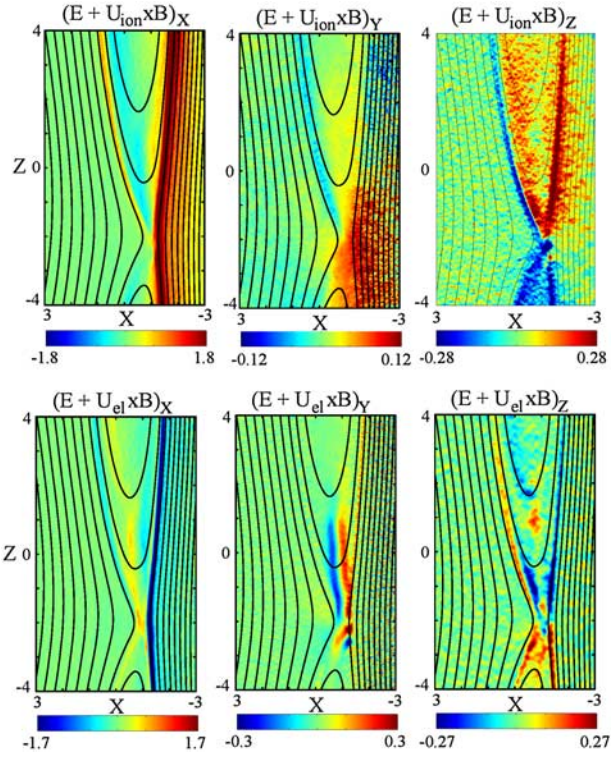


**Figure 3.** Components of $\mathbf{E} + \mathbf{U}_I \times \mathbf{B}$ and $\mathbf{E} + \mathbf{U}_e \times \mathbf{B}$. The red and blue regions in each plot are the locations where the magnitude of the quantity of interest is greater than half of its peak value.

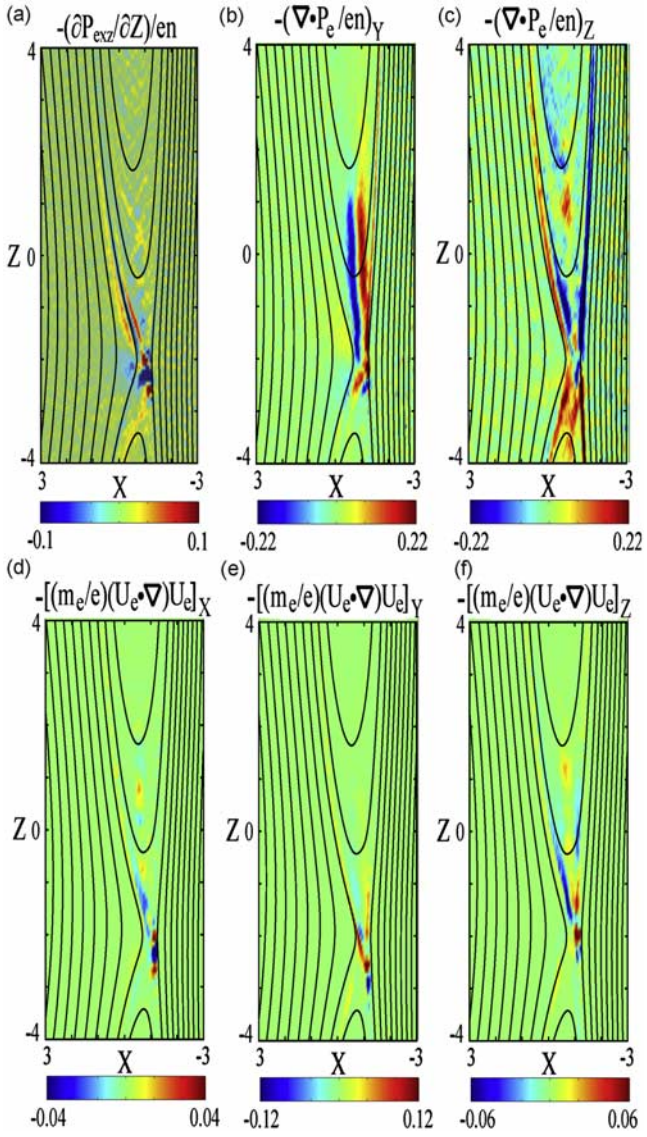


**Figure 4.** Components of $-\nabla \cdot \mathbf{P}_e/en$ and $-(m_e/e)(\mathbf{U}_e \bullet \nabla)\mathbf{U}_e$). The red and blue regions in each plot are the locations where the magnitude of the quantity of interest is greater than half of its peak value.

regions do not exactly overlap the parallel electric field regions, electromagnetic energy conversion is produced by both perpendicular and parallel currents and fields. Near the X-line and on electron scales, the parallel electric field contributes significantly to the electromagnetic energy conversion while, averaged over the simulation volume, it is associated with about 10% of the conversion because $\mathbf{j}_{perp}\mathbf{E}_{perp}$ accounts for the rest.

[13] The parallel electric field of a few mV/m, extending over about one ion skin depth in Figure 1a, produces ~100 volts of field aligned electric potential so it may be important for accelerating the quasi-monoenergetic field aligned electron beams that have been observed on the magnetospheric side of the current sheet and in the magnetosphere [*Mozer et al.*, 2005].

[14] The red and blue colors in Figure 1c give the regions where the Z-component of the electron flow has a magnitude that exceeds half of the peak value of about 2.8 normalized units. This may be compared with the electron flow speed in the out-of plane direction of 6.25 normalized units (see Figure 2f). Large Z-directed flows occur along the separatrices over the entire length of the simulation with widths the order of the electron skin depth. In addition, there is a large outflow through the center of the magnetopause in the northern hemisphere. This north-south asymmetry has been discussed earlier [*Mozer et al.*, 2008; *Pritchett*, 2008] and it results from a non-zero guide magnetic field whose spatial variation is different in the two hemispheres. This flow extends in the Z-direction over about four ion skin depths, after which it slows to become the order of the ion Alfven speed. It does not exactly coincide in space with either the parallel electric field region or the electromagnetic energy conversion region. For symmetric reconnection, this outflow has been found to occur in both hemispheres over many tens of ion skin depths in the outflow direction [*Karimabadi et al.*, 2007; *Phan et al.*, 2007; *Shay et al.*, 2007; *Ji et al.*, 2008]. Figure 1d presents the electron beta. In the vicinity of $E_{||}$, the beta value is 0.3 to 3, i.e., not generally much greater than one.

[15] Figure 3 presents the three components of $\mathbf{E} + \mathbf{U}_I \times \mathbf{B}$ in the top row and the three components of $\mathbf{E} + \mathbf{U}_e \times \mathbf{B}$ in the bottom row. The extended blue and red surfaces in these plots cover regions where ideal MHD does not apply by a significant amount over a significant region of space. The X-components of these colored surfaces for both the ions and electrons extend to the limits of the 25.6 $c/\omega_{pI}$ simulation. It is noted that the X-components in the first column dominate the other components in magnitude and that the sign of $(\mathbf{E} + \mathbf{U}_I \times \mathbf{B})_X$ is opposite to that of $(\mathbf{E} + \mathbf{U}_e \times \mathbf{B})_X$. This difference of sign is considered by examining the components of equations (2) and (3) where the values below these re-written equations give the X-components of the several terms in each equation at Z = −2.28 and X = −1.37, in mV/m for $B_0$ = 45 nT and $n_0$ = 10 $cm^{-3}$. This location is included in Figure 2.

| $E_X$ | $(\mathbf{U}_I \times \mathbf{B})_X$ | = | $(\mathbf{j} \times \mathbf{B}/en)_X$ | $(-\nabla \cdot \mathbf{P}_e/en - (m_e/e)[\partial \mathbf{U}_e/\partial t + (\mathbf{U}_e \bullet \nabla)\mathbf{U}_e])_X$ | | LHS | RHS |
|---|---|---|---|---|---|---|---|
| 35 | 2 | = | 85 | − 46 | small | − 1 | 37 | 38 |

| $E_X$ | $(\mathbf{U}_e \times \mathbf{B})_X$ | = | $(-\nabla \cdot \mathbf{P}_e/en - (m_e/e)[\partial \mathbf{U}_e/\partial t + (\mathbf{U}_e \bullet \nabla)\mathbf{U}_e])_X$ | | | LHS | RHS |
|---|---|---|---|---|---|---|---|
| 35 | − 84 | = | −46 | small | − 1 | − 49 | − 47 |

Because the derivatives associated with the terms on the right side of the Generalized Ohm's Law are obtained from finite differences of rapidly varying quantities, they under-

estimate the true magnitudes of these quantities. To compensate for this, the terms on the left side of the Generalized Ohm's Law and in Figure 3 represent the averages of the data over a normalized interval of 0.1 by 0.1 units, which corresponds roughly to one electron skin depth by one electron skin depth. This averaging reduces the peak magnitudes by 10–20%. The partial derivative with respect to time in the above expressions has not been estimated because it is negligible compared to the other terms. The relativistic correction to the electron mass must be included in a quantitative estimate of the pressure and inertia terms because c is about 20 times the Alfven speed.

[16] Figure 4 presents the three components of the pressure (Figures 4a–4c) and inertia (Figures 4d–4f) terms using a color scale that saturates at half of the peak amplitude in each plot such that the blue and red regions are those having magnitudes within a factor of two of the maximum of that component. The X-component of $-\nabla \cdot \mathbf{P}_e$ is the sum of $-\partial P_{exx}/\partial x$ and $-\partial P_{exz}/\partial z$. Because $\partial P_{exx}/\partial x$ does not contribute to a parallel electric field that satisfies equation (1), at least in the two-dimensional idealized case, it does not contribute to reconnection. Thus, $-(\partial P_{exz}/\partial z)/en$ is plotted in place of $-(\nabla \cdot \mathbf{P}_e/en)_X$ in Figure 4a. ($-\partial P_{exx}/\partial x$ dominates the other terms in Figure 4 by an order-of-magnitude.) It is noted that the three plotted components of the pressure divergence term are comparable and are important over spatial scales of several ion skin depths. The inertia terms in the bottom row are generally a factor of 2–4 smaller than the pressure terms but they are not negligible.

## 4. Summary

[17] Regions associated with electron physics in asymmetric magnetic field reconnection with a guide magnetic field have been examined to show that they do not completely overlap, are not confined in all dimensions to sizes the order of the electron skin depth, do not surround the X-line, and are not embedded in a larger region where the ion ideal MHD is violated. There is good agreement between space and simulation observations of the flows and fields in these electron physics regions. The inertia and pressure terms on the right side of the Generalized Ohm's Law are non-zero over large regions.

[18] Parallel electric fields are required for reconnection to occur but their existence is not a sufficient condition that reconnection is occurring. Near the X-line and on electron scales, these parallel electric fields contribute significantly to the electromagnetic energy conversion while, averaged over the simulation volume, they are associated with ~10% of the conversion. Thus, the large scale perpendicular electric field is the source of most of the total particle energization during reconnection. The north-south asymmetry associated with asymmetric reconnection with a guide magnetic field results in more important electron and ion flows into the exhaust region from one hemisphere than the other. The electron exhaust jet exists over a shorter length for asymmetric reconnection with a guide field than it does for symmetric reconnection, at least in this simulation.

[19] The present simulation results have confirmed the presence in asymmetric reconnection of electron physics on ion spatial scales in which $(\mathbf{E} + \mathbf{U}_e \times \mathbf{B}) \neq 0$ and important pressure divergences and significant inertia terms exist. These results are in excellent agreement with previous in-situ observations [*Mozer*, 2005] and serve as encouragement for the success of the upcoming NASA Magnetospheric Multi-Scale mission, which has as a main objective the detailed study of these regions.

[20] **Acknowledgments.** This research was supported by NASA grants NNX08AM15G, NNG05GL27G, and NNG05GC72G and contract NAS5-02099-07/09. The particle simulations were performed using resources of the San Diego Supercomputer Center (supported by the National Science Foundation under cooperative agreement ACI-9619020) and the UCLA Dawson Cluster (funded by NSF grant PHY-0321345).

## References

Ji, H., Y. Ren, M. Yamada, S. Dorfman, W. Daughton, and S. P. Gerhardt (2008), New insights into dissipation in the electron layer during magnetic reconnection, *Geophys. Res. Lett.*, *35*, L13106, doi:10.1029/2008GL034538.

Karimabadi, H., W. Daughton, and J. Scudder (2007), Multi-scale structure of the electron diffusion region, *Geophys. Res. Lett.*, *34*, L13104, doi:10.1029/2007GL030306.

Longmire, C. L. (1963), *Elementary Plasma Physics*, John Wiley Intersci., New York.

Mozer, F. S. (2005), Criteria for and statistics of electron diffusion regions associated with subsolar magnetic field reconnection, *J. Geophys. Res.*, *110*, A12222, doi:10.1029/2005JA011258.

Mozer, F. S., S. D. Bale, T. D. Phan, and J. A. Osborne (2003), Observations of electron diffusion regions at the subsolar magnetopause, *Phys. Rev. Lett.*, *91*, 245002, doi:10.1103/PhysRevLett.91.245002.

Mozer, F. S., S. D. Bale, J. P. McFadden, and R. B. Torbert (2005), New features of electron diffusion regions observed at subsolar magnetic field reconnection sites, *Geophys. Res. Lett.*, *32*, L24102, doi:10.1029/2005GL024092.

Mozer, F. S., P. L. Pritchett, J. Bonnell, D. Sundkvist, and M. T. Chang (2008), Observations and simulations of asymmetric magnetic field reconnection, *J. Geophys. Res.*, *113*, A00C03, doi:10.1029/2008JA013535.

Newcomb, W. A. (1958), Motion of magnetic lines of force, *Ann. Phys.*, *3*, 347–385.

Phan, T. D., J. F. Drake, M. A. Shay, F. S. Mozer, and J. P. Eastwood (2007), Evidence for an elongated (>60 ion skin depths) electron diffusion region during fast magnetic reconnection, *Phys. Rev. Lett.*, *99*, 255002, doi:10.1103/PhysRevLett.99.255002.

Pritchett, P. L. (2008), Collisionless magnetic reconnection in an asymmetric current sheet, *J. Geophys. Res.*, *113*, A06210, doi:10.1029/2007JA012930.

Shay, M. A., J. F. Drake, and M. Swisdak (2007), Two-scale structure of the electron dissipation region during collisionless magnetic reconnection, *Phys. Rev. Lett.*, *99*, 155002, doi:10.1103/PhysRevLett.99.155002.

Vasyliunas, V. M. (1975), Theoretical models of magnetic field line merging, 1, *Rev. Geophys.*, *13*, 303–336.

F. S. Mozer, Space Sciences Laboratory, University of California, Berkeley, CA 94720, USA. (fmozer@ssl.berkeley.edu)

P. L. Pritchett, Department of Physics and Astronomy, University of California, Los Angeles, CA 90095-1547, USA.